Galaxy Peculiar Velocities and Infall onto Groups

M. L. Ceccarelli, C. Valotto, D. G. Lambas
IATE, Observatorio Astronómico, Universidad Nacional de Córdoba, Laprida 854, Córdoba 5000, Argentina; laura@mail.oac.uncor.edu

N. Padilla
Departamento de Astronomía y Astrofísica, Pontificia Universidad Católica de Chile, Vicuña Mackenna 4860, Santiago, 22, Chile.

R. Giovanelli and M. Haynes
Department of Astronomy, Space Sciences Building, Cornell University, Ithaca, NY 14853

ABSTRACT

We perform statistical analyses to study the infall of galaxies onto groups and clusters in the nearby Universe. The study is based on the Updated Zwicky Catalog and Southern Sky Redshift Survey 2 group catalogs and peculiar velocity samples. We find a clear signature of infall of galaxies onto groups over a wide range of scales 5 h^{-1} Mpc< r < 30 h^{-1} Mpc, with an infall amplitude on the order of a few hundred kilometers per second. We obtain a significant increase in the infall amplitude with group virial mass (M_V) and luminosity of group member galaxies (L_g). Groups with $M_V < 10^{13}$ $M_\odot$ show infall velocities $V_{infall} \simeq 150$ km s^{-1} whereas for $M_V > 10^{13}$ $M_\odot$ a larger infall is observed, $V_{infall} \simeq 200$ km s^{-1}. Similarly, we find that galaxies surrounding groups with $L_g < 10^{15}$ $L_\odot$ have $V_{infall} \simeq 100$ km s^{-1}, whereas for $L_g > 10^{15}$ $L_\odot$ groups, the amplitude of the galaxy infall can be as large as $V_{infall} \simeq 250$ km s^{-1}. The observational results are compared with the results obtained from mock group and galaxy samples constructed from numerical simulations, which include galaxy formation through semianalytical models. We obtain a general agreement between the results from the mock catalogs and the observations. The infall of galaxies onto groups is suitably reproduced in the simulations and, as in the observations, larger virial mass and luminosity groups exhibit the largest galaxy infall amplitudes. We derive estimates of the integrated mass overdensities associated with groups by applying linear theory to the infall velocities after correcting for the effects of distance uncertainties obtained using the mock catalogs. The resulting overdensities are consistent with a power law with $\delta \sim 1$ at $r \sim 10h^{-1}Mpc$.

Subject headings: galaxies: infall – galaxies; peculiar velocities – galaxy group: spherical collapse

1. Introduction

Inhomogeneities in the distribution of matter are the source of peculiar velocities in the universe. The nature of this velocity field depends on the local density. High density regions show a collection of random motions typical of virialized objects whereas, low density environments, on the other hand, are more likely to show streaming motions: objects falling towards larger potential wells constantly increasing the amplitude of their clustering strength (Diaferio & Geller, 1997).

A possible model for describing the dynamical behavior of objects near regions of high density contrast is provided by the spherical infall model (for a discussion see Tolman, 1934; Gunn & Gott, 1972; Silk, 1974; Elkolm & Teerrikorpi, 1994). This model simplifies the problem by assuming that the initial density perturbation responsible for the formation of an object is spherically symmetric. The gravitational field around this perturbation traces the symmetry of the matter, and its pull induces peculiar motions over the surrounding area. Here the velocity field takes the form of a collapsing streaming motion towards the local density maximum. In the linear perturbation case, the infall velocity (V_{infall}) depends on the distance to the local density maximum and is directly related to the density contrast (Peebles, 1980),

$$V_{infall} = -(1/3)\Omega_0^{0.6} H_0 r \delta(r) \tag{1}$$

In high density regions, as is the case of neighborhoods of clusters and galaxy groups, linear theory is not expected to provide an adequate description (Croft et al. 1999). However, if we assume that mass overdensities are spherically symmetric, an approximate solution for the non-linear collapse can be found. This solution treats the overdensity as an isolated Friedmman universe with its own value of Ω_0 (for more details see Gunn & Gott, 1972; Bondi, 1974; Silk, 1974; Gunn, 1978; Rëgos & Geller, 1989 and references therein). For these non-linear regions, the relation for linear collapse is replaced by an approximate solution (Yahil, 1985). This solution has shown to give accurate results outside the virialized regions of groups and clusters of galaxies.

In this work we investigate the structure of the peculiar velocity field around groups of galaxies in the nearby universe. We apply the spherical infall model to test the effects of overdensities in the density field, traced by groups of galaxies, on the dynamical properties of their surrounding regions.

This paper is organized as follows. In section 2 we present the observational data samples used to perform the statistical analyses. We describe the semi-analytic mock catalogs in

section 3. Section 4 contains the description of the statistical methods adopted to obtain the results shown in sections 5 and 6. In section 7 we show the results of the method described in section 3 applied to the mock catalogs. In section 8 we apply a correction factor to consider distance uncertainties on the amplitude of infall velocities and we use these estimates to predict the integrated mass overdensity associated to groups from linear theory. Finally, we make a brief discussion of the results.

2. Observational Data

In this section we describe in detail the observational samples used in this paper. We use two different sets of data. The first set is composed of tracers of the density peaks, which in this work are galaxy groups from the Updated Zwicky Catalog (UZC; Merchán et al. 2000) and the Southern Sky Redshift Survey (SSRS2). The second set of data contains galaxy peculiar velocity information taken from the compilation of Giovanelli and Haynes (2002, hereafter CPV), which we use to investigate the velocity field around mass concentrations.

We use the UZC group catalog constructed by Merchán et.al (2000). These groups were identified from the UZC galaxy catalog (Falco et al. 1999) which contains 19,369 galaxies with apparent Zwicky magnitudes $m_{Zw} \leq 15.5$ and with a 96% completeness in redshift. The region covered by the catalog is bounded by $20^h \leq \alpha_{1950} \leq 4^h$, $8^h \leq \alpha_{1950} \leq 17^h$ and $-2.5^o \leq \delta_{1950} \leq 90^o$, providing accurate coordinates within 2" and reliable redshifts in the range $cz = 0 - 25,000$ km s^{-1}, with a reasonably complete sky coverage (see Falco et al. 1999 for more details). The algorithm adopted by Merchán et al. (2000) for the construction of the group catalog follows the basic procedure described by Huchra & Geller (1982) with the improvements introduced by Maia et al. (1989) and Ramella et al. (1997) that minimize the number of interlopers. The group inner regions have a density contrast relative to the mean density of galaxies $\delta\rho/\rho = 80$. The UZC group catalog (GUZC) contains systems with at least four members and mean radial velocities, $V_{gr} \leq$ 15,000 km s^{-1} comprising a total number of 513 groups.

The top half of figure 1 shows the angular distribution of the CPV galaxies and UZC groups. As can be seen, these objects are all concentrated on the northern hemisphere, with a sampling rate that does not present important variations across the solid angle covered.

We also use groups identified from the SSRS2 catalog (Da Costa et al. 1998) which comprises 5369 objects with apparent B magnitudes $m_B \leq 15.5$. The region covered is 1.70 sr in the southern celestial hemisphere providing accurate coordinates within 1". This catalog of groups was constructed using the same algorithm used for the GUZC (Merchán,

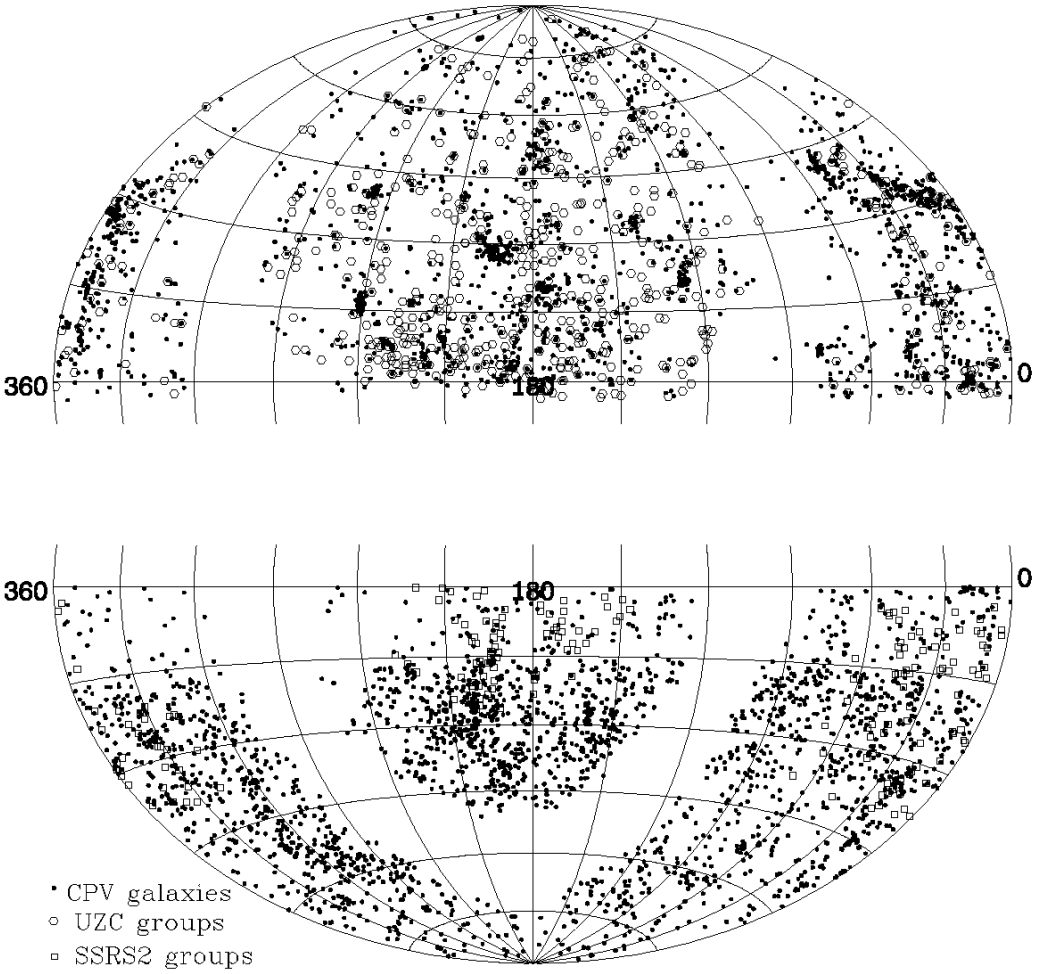

Fig. 1.— Top: Angular distribution of north CPV galaxies (points) and UZC groups (hexagons) for the northern hemisphere in equatorial coordinates. Bottom: Angular distribution of south CPV galaxies (points) and SSRS2 groups (open squares) for the southern hemisphere, also in equatorial coordinates

2000). The SSRS2 group catalog contains systems with a minimum of four members and mean radial velocities, $V_{gr} \leq 15{,}000$ km s^{-1} , comprising a total of 386 groups. The bottom half in figure 1 shows the angular positions of groups from the SSRS2 and CPV southern galaxies.

2.1. Peculiar velocity data

Peculiar velocities have been derived for 4452 galaxies using I-band photometry and either optical long slit spectroscopy or global HI profiles (e.g. Dale & Giovanelli 2000). The sample includes objects in the Haynes *et al.* (1999), Mathewson & Ford (1996) and Giovanelli *et al.* (1997a) compilations, as well as more recently processed data, the public presentation of which is in preparation by our group. Widths derived from optical rotation curves follow the method outlined in Giovanelli & Haynes (2002). Peculiar velocities were derived using the template relation and the derivation technique presented in Giovanelli *et al.* (1997b). Analyses of the large–scale flow properties of the peculiar velocity field based on these samples are summarized in Dale & Giovanelli (2000).

3. Mock Catalogues with Semi-analytic Models of Galaxy Formation

In order to compare model predictions to observational results we use mock catalogs extracted from a high resolution N-body simulation populated with galaxies using the semi-analytic model `GALFORM` (Cole et al. 2000; Benson et al. 2002), by the Theory Group at the University of Durham. The numerical simulation uses standard ΛCDM parameters, a normalization $\sigma_8 = 0.80$, and a primordial spectral index of $n = 0.97$, in agreement with the constraints from the first year of data from WMAP (Spergel et al. 2003). The N-body simulation box is $250h^{-1}$ Mpc on a side and contains 1.25×10^8 dark matter particles of mass $1.04 \times 10^{10} h^{-1} M_\odot$. Dark matter halos are identified in the $z = 0.$ output using a friends of friend method and rejecting those halos with less than 10 particles. As a result, the halo resolution limit is $1.04 \times 10^{11} h^{-1} M_\odot$. The procedure followed by the Durham group for populating the dark matter halos follows the technique described by Benson et al. (2002). Essentially, the `GALFORM` code is run for each halo, and galaxies are assigned to a subset of dark matter particles in the halo. Around 90% of central galaxies brighter than $M_{b_J} - 5 \log_{10} h = -17.5$ are expected to be in halos resolved by the simulation. The effective limit of the catalog was extended to $M_{b_J} - 5 \log_{10} h = -16$ using a separate `GALFORM` calculation for a grid of halo masses below the resolution limit of the N-body simulation. These galaxies are assigned to particles that are not identified as part of a dark matter halo.

First, we investigate the infall of mass particles onto the dark matter halos in the numerical simulation. Figure 2 shows the mean infall velocity of dark matter particles and semianalytic galaxies in the simulation cube as a function of distance to the halo center of mass. We show results for the full sample of semianalytic galaxies and for those with $B_j < -18$. This figure shows in different shades of gray, results for subsamples of halos defined using different lower mass limits. As can be seen, galaxies show a similar infall velocity to dark matter particles even when they are restricted to brighter galaxies. The infall velocities seem to be marginally lower for galaxies than for the dark matter.

In a second step, we extract mock catalogs from the numerical simulation. These play a fundamental role in our analysis. We use them to tailor our algorithms to extract the maximum streaming motion signal and to asses random and systematic errors in our calculations. We estimate systematic errors by comparing the results measured from the mock catalogs with the results from measuring the streaming motions in the simulation cube. Random errors are calculated by the dispersion of streaming motions measured from each individual mock galaxy around the mean infall velocities from all the mock galaxies.

Mock UZC and SSRS2 are constructed by placing an observer at a random location within the simulation box and applying the radial and angular selection function of the UZC and SSRS2, respectively. We also assign each mock galaxy a morphological type, which is assumed to be a function of the stellar formation rate (SFR; high SFR corresponds to late types, low SFR to early types). The group finding algorithm is applied to the galaxy mock catalog in the same way as for the real data to construct a mock group catalog that mimics UZC groups. In order to obtain a CPV mock catalog we take account the fact that CPV data comprise mainly late-type galaxies, so we apply a further constraint to account for this in our mock galaxy sample by restricting it to late types. Finally, we also impose the radial velocity distribution of CPV galaxies to this sample (see figure 3).

In addition, the mock catalogs are selected so as to reproduce the local group velocity with respect to the cosmic microwave background and also the surrounding structures, which consist mainly of reasonably important filaments aligned with the observer's line of sight to ≈ 30 degrees.

Figure 3 shows the number of CPV galaxies as a function of redshift $[N(z)]$. In the figure, the mock redshift distribution is shown as a dashed histogram and the real data of $N(z)$ are shown as a solid histogram.

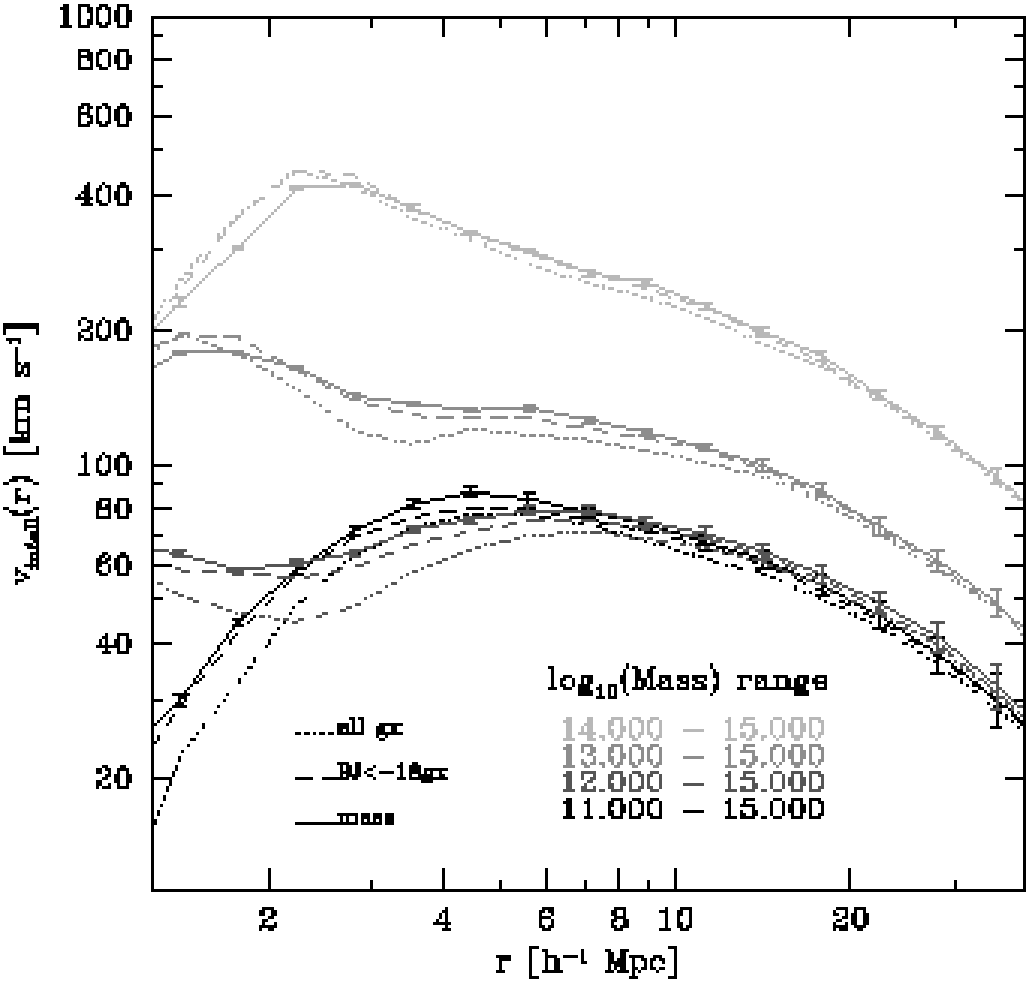

Fig. 2.— Mean infall velocity of particles in the LCDM simulation (solid lines) and galaxies (all semianalytic galaxies: dotted lines; galaxies such that $B_j < -18$: dashed lines) as a function of radial distance to the center of mass of the groups.

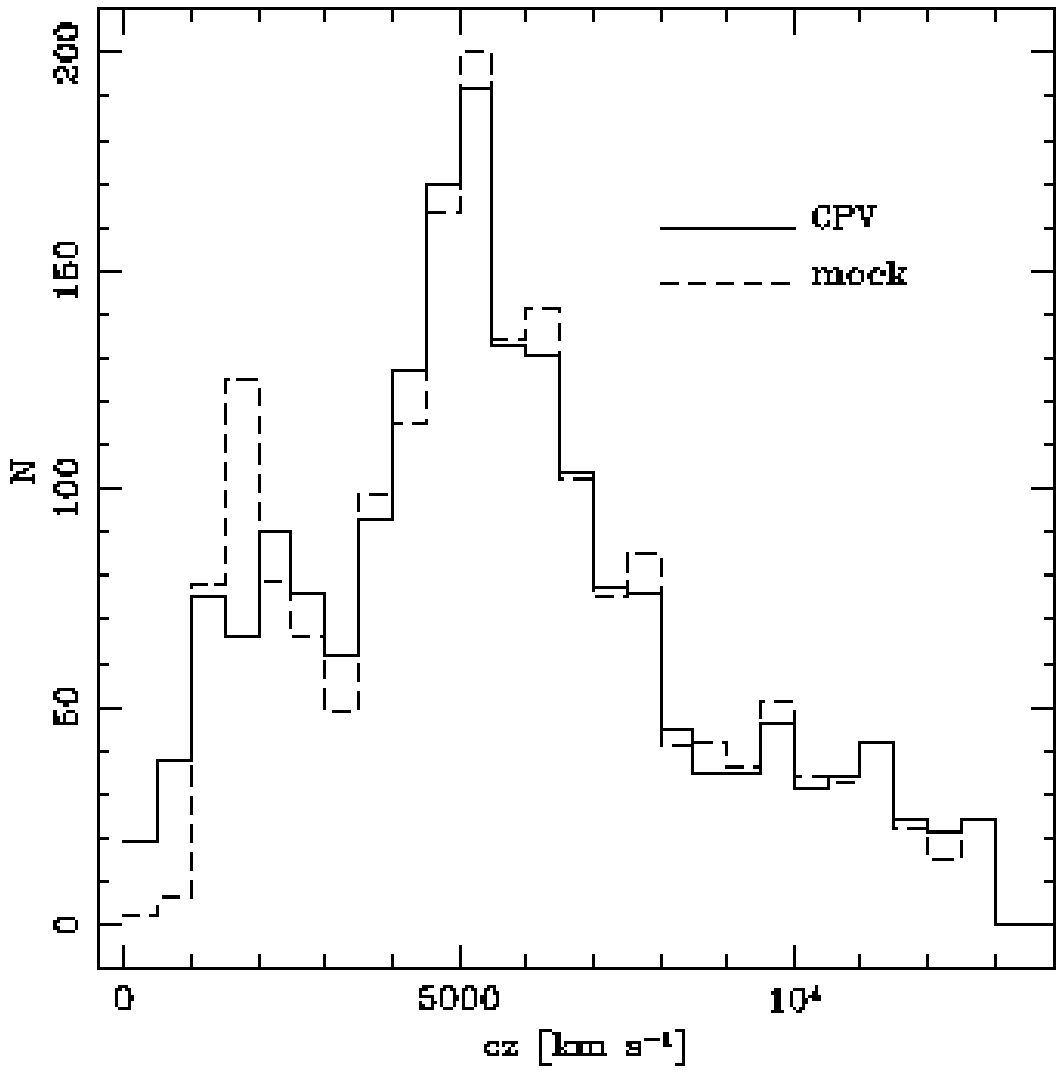

Fig. 3.— Radial velocity distribution of CPV galaxies (solid histogram) and mock CPV galaxies (dashed histogram)

4. Statistical Methods

In this work, we analyse the statistical properties of galaxy peculiar velocities in the neighborhoods of galaxy groups. Galaxies are considered to be test particles under the gravitational action of a spherically symmetric overdensity in the matter distribution, traced by the positions of galaxy groups.

The infall model provides a description for the radial collapse of galaxies towards higher density regions. We expect this model to be a good approximation to the actual dynamics in the local universe, with a less important tangential component in the streaming motions of galaxies. In this analysis we will assume the motions are only radial.

We can find the mean infall of galaxies onto groups and clusters using galaxy peculiar velocities, which give only the line-of-sight projection of the three-dimensional velocity vector. The effect of this projection can be described in a simple way as a function of the galaxy position relative to both the group center and the observer by the linear relation

$$V_r(r,\theta) = V_{infall}(r)\cos(\theta), \tag{2}$$

where θ is the angle subtended by the observer and the galaxy as seen from the group center. We have neglected in this analysis group peculiar velocities whose effects are expected to cancel out in this statistical study.

We analyse the dependence of galaxy peculiar velocities, V_{pr}, on $\cos(\theta)$ in different spherical concentric shells around the individual groups and calculate averages $< V_{pr}(\theta) >$ and its standard mean deviation $\sigma_{V_{pr}}$ for different bins in $\cos(\theta)$ for the total group sample.

In order to enhance the statistical significance of our results we adopt an iterative process by which we repeatedly calculate $< V_{pr} >$ from a reduced sample of galaxies. The reduced sample is constructed by removing all the galaxies which lie at more than $2\sigma_{V_{pr}}$ from the mean linear relation calculated from the sample of galaxies used in the previous iteration. We adopt four iterations, which is enough to stabilize the results.

The mean infall amplitude $V_{infall}(r)$ as a function of scale r is derived from least-squares linear fitting applied to the observed $< V_{pr} >$ versus $cos\theta$ measured on shells of radius r around the groups. Then $V_{infall}(r)$ is simply the slope of the line fitted to the data (see equation 2).

5. Analysis and Results

In order to analyze the dynamical properties of CPV galaxies we have selected groups in the radial velocity range $2,000$ km s$^{-1} < cz < 8,000$ km s^{-1}. We define concentric spherical shells around each group in our samples and identify the galaxies that lie in them. Once we do this, we can calculate the angle θ subtended by the directions to the galaxy and the observer from the center of the group.

In figure 4 we show the mean projected peculiar velocity as a function of θ bins for the CPV galaxies and UZC groups. The different panels correspond to spherical shells of different radii r. As can be seen in the figure, there is an important variation of $V_{infall}(r)$ with shell radius. In this figure, errors are derived from the scatter of measurements obtained from the data. At small r, the errors are larger than the mean peculiar velocity because galaxies do not follow radial trajectories near the center of the groups (panel a). In the external regions errors become smaller and the infall motions show stable values over a wide range of distances. The maximum in infall amplitude occurs at 5 h^{-1} Mpc $< r <$ 30 h^{-1} Mpc; at these scales the predominant motions are aligned with the radial direction (panels b, c and d). At scales $r >$ 30 h^{-1} Mpc, the influence of surrounding structures starts to affect the values of infall velocities (panels e and f), which become consistent with values $\sim$ 0km s^{-1}, because of the large error bars.

We repeat this analysis using groups and galaxies in the southern hemisphere and show in figure 5 the resulting values of streaming motions V_{infall} for both the SSRS2 and UZC galaxies (from the southern and northern hemisphere respectively) and for the combined set of samples (north and south). The solid line in the figure 5 summarizes the results shown in figure 4. Here each point corresponds to the slope of the lines fitted in each panel of 4, and errors represent the scatter of results from individual mock catalogs around their mean (see section 3). As can be seen in figure 5, there is a clear indication of infall motions outside the virialized regions. At the largest radius the infall signal is negligible, an expected effect caused by the action of the gravitational pull of neighboring groups. The results are similar for both hemispheres.

6. Dependence on Virial Mass and Group Luminosity

Once we have a direct detection of the infall of galaxies onto groups, we can study possible dependencies of the amplitude of infall velocities on group properties. It is expected that the amplitude of the infall velocities increases with group mass. In order to test this assumption we must obtain estimates of the group masses. This can be achieved by two

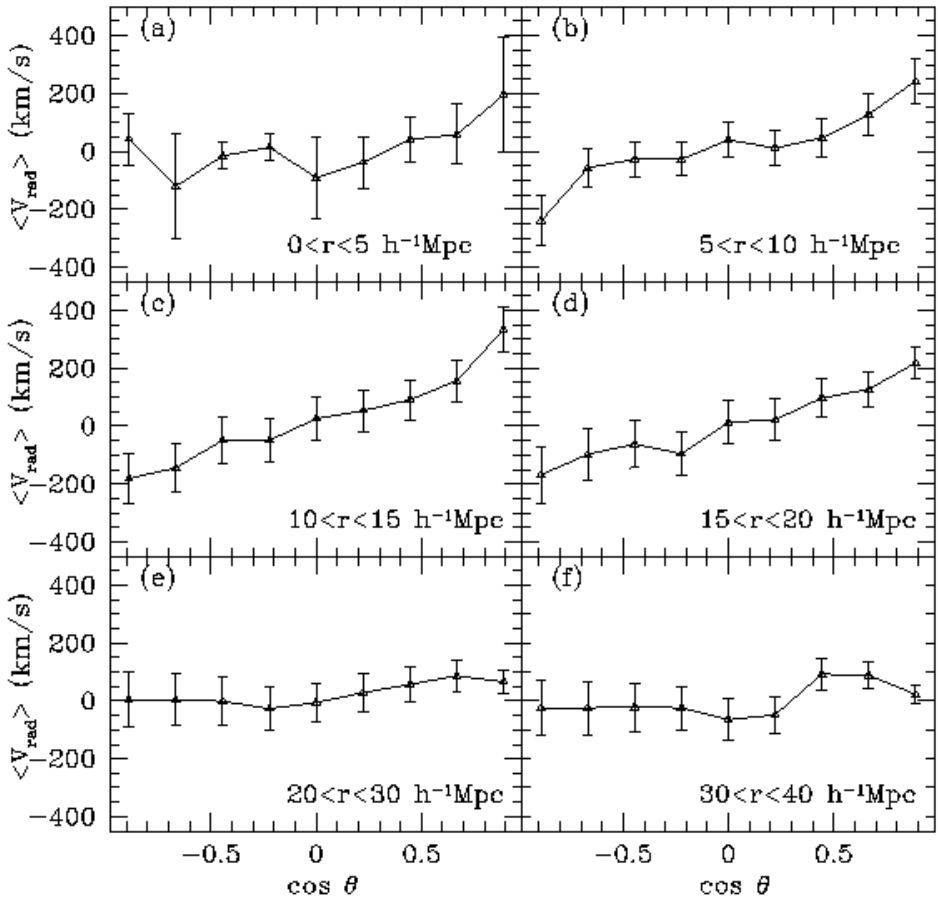

Fig. 4.— Mean values $< V_{pr} >$ as a function of the angle θ subtended by the group-galaxy and group-observer directions for the CPV galaxies and UZC groups. The units of r are h^{-1} Mpc. The different panels correspond to different distances to the group center: (a) $0 < r < 5$; (b) $5 < r < 10$; (c) $10 < r < 15$; (d) $15 < r < 20$; (e) $20 < r < 30$; (f) $30 < r < r40$

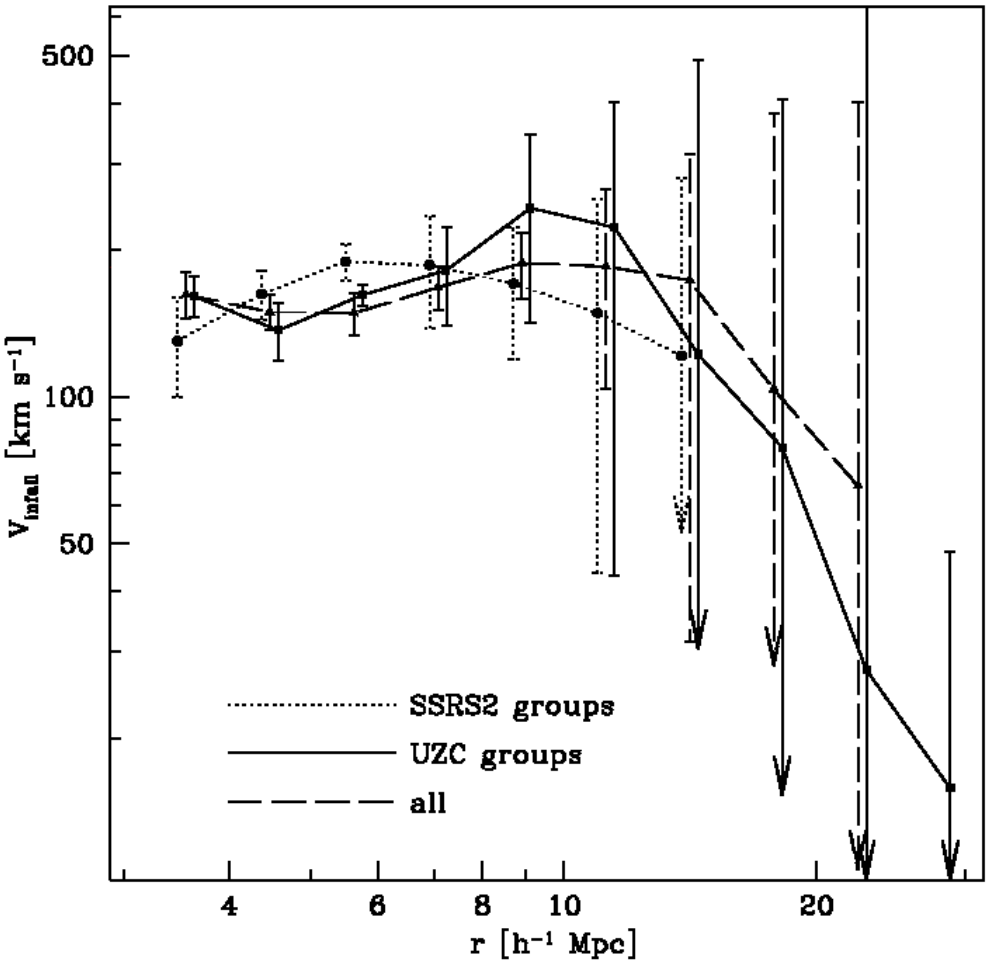

Fig. 5.— Mean streaming motions of CPV galaxies onto UZC groups in northern hemisphere (solid line), SSRS2 groups in southern hemisphere (dotted line), and the combined data set (dashed line). Errors are calculated using mock catalogs.

independent methods. The first approach is to compute the group virial mass which in spite of having the advantage of being a direct estimate, is subject to significant uncertainties mainly due to small number statistics. A second approach is to estimate group masses by measuring the total luminosity of group member galaxies. This method can provide a suitable estimate of the group mass by assuming a constant M/L relation and is less unstable regarding small number statistics (Padilla et al. 2004, Eke et al. 2004). We have considered the dependence of the amplitude of infall on group luminosity. We estimate group luminosities in the m_{Zw} band by adding up galaxy luminosities from the UZC catalog that are within 1.5 h^{-1} Mpc from the group center, with a relative velocity $\Delta V < 500$ km s^{-1}. This provides a rough estimate of the groups total luminosity and serves as an adequate procedure to deal with two subsamples of different total luminosities. These subsamples are constructed such that they contain similar numbers of groups.

In figure 6 we show the resulting infall velocities derived from the two group subsamples subdivided by luminosity ($L_g > 10^{15}$ $L_\odot$ and $L_g < 10^{15}$ $L_\odot$). As can be seen, there is a remarkable difference between the infall amplitude of both subsamples. We also show in figure 6 the infall onto subsamples of groups subdivided according to virial masses ($M_V > 2\times10^{13}$ $M_\odot$ and $M_V < 2\times10^{13}$ $M_\odot$). As in the case in which we define our subsamples using group luminosities, the subdivision by mass is set so that both subsamples contain nearly equal numbers.

By inspection to figure 6, it can be seen that by subdividing the sample by luminosity, the difference in the amplitude of infall velocities is larger than by subdividing the sample by virial mass. This larger dependence of the amplitude of infall on group luminosity with respect to virial mass may reflect the fact that the latter might be more subject to large uncertainties than estimates of mass derived from luminosity, in agreement with Padilla et al. (2004) and Eke et al. (2004).

7. Results from the Mock Catalogs

We calculate the mean streaming peculiar velocity towards simulated groups for galaxies in the mock catalogs by using the same methods that we applied to the observational data. In panel a) of figure 7 we show the mean infall motions (averaged over seven mock catalogs) for two subsamples of groups per mock catalog defined by two different lower limits in dynamical mass. We find that in scales ranging from 5 to 30 h^{-1} Mpc the predominant motion occurs preferentially in the radial direction. Closer to the group centers, errors in V_{infall} (calculated from the scatter among seven mock catalog) grow larger as virialized motions start to dominate the galaxy velocities. At large separations, the infall signal disappears,

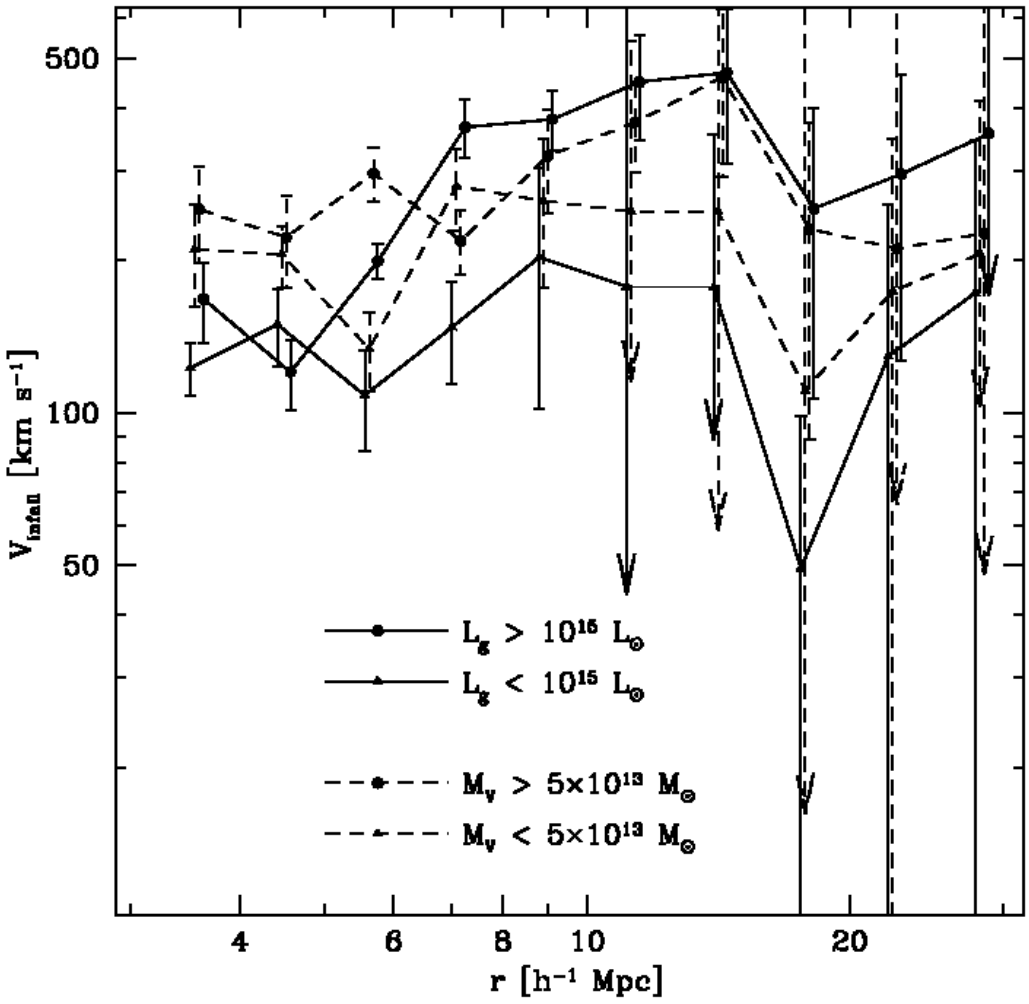

Fig. 6.— Mean infall velocity onto samples in UZC galaxy groups. Solid lines indicate luminosity subsamples, and dashed lines indicate virial mass subsamples. Errors are derived from the scatter of measurements from several mock catalogs.

probably because of the effect of neighboring groups. The results obtained from the mock samples are at least in qualitative agreement with the observational data.

The resulting average infall velocities recovered from the mock catalogs and thosse measured directly from the simulation box are comparable. For instance, at separations of 10 h^{-1}Mpc, the values of infall are 60 ± 20km/s and 62 ± 2km/s for the mock and cube data, respectively, for halos with $M > 10^{11}h^{-1}M_{\odot}$. In the case of the most massive halos with $M > 10^{14}h^{-1}M_{\odot}$, the infall velocities become 100 ± 30km/s and 210 ± 3 km/s, respectively. As a note of caution, one should therefore bear in mind that the relation between infall amplitude and halo mass seems to be slightly less step when measured from the mock catalogs, which show consistent infall amplitudes for the low-mass halos and lower amplitudes for the high-mass halos than the true underlying value.

Up to this point, peculiar velocities in the mock catalogs were not affected by measurement errors. We apply a distance measurement error proportional to the distance to the galaxies similar to the one that affects the observational data. We consider an uncertainty of 20% in the distance measurement, repeat the calculation of infall velocities for the mock catalogs, and show the results in panel b of figure 7. By comparing this panel to panel a) and panel c) which show the infall motions for the mock catalog without errors and for the UZC data, respectively, it can be seen that errors in distance measurementes bring the results from synthetic data closer to the observational data. In order to correct for the effect of distance uncertainties in the inferred infall velocities, we compare the results from the mock catalogs with and without distance errors. We calculate the ratio $f = V_{mock-errors}/V_{mock}$, where $V_{mock-errors}$ is the infall amplitude of the mock catalogs with distance errors (see panel b in figure 7) and V_{mock} is the infall amplitude from the mock catalogs without distance errors (see panel a in figure 7). Panel a of figure 8 shows f for different scales and a fitting function of the form $f = a + br/(h^{-1}Mpc) + clog(r(h^{-1}Mpc))$, which is sufficient to provide a good description of the ratio of observed to actual velocities. We find that a=2.4, b=0.125, and c=-1.94 provide a good fit to the measured values of f.

As it can be seen in this figure, the correction factor f increases slightly with scale, with a mimimun value $f \simeq 1.5$ at $3h^{-1}Mpc$ and $f \simeq 2.8$ at $20h^{-1}Mpc$. Thus, in order to obtain realistic estimates, all the inferred infall velocities should be reduced by these values.

We note, however, that the resulting infall velocities do not depend significantly on the particular function adopted to fit the correction factor f. Panel b in figure 8 shows the corrected mean amplitude for two ranges in group virial mass. We note that the lower values of the corrected infall velocities are in suitable agreement with those shown in figure 2 for mass and galaxies in the Λ CDM model.

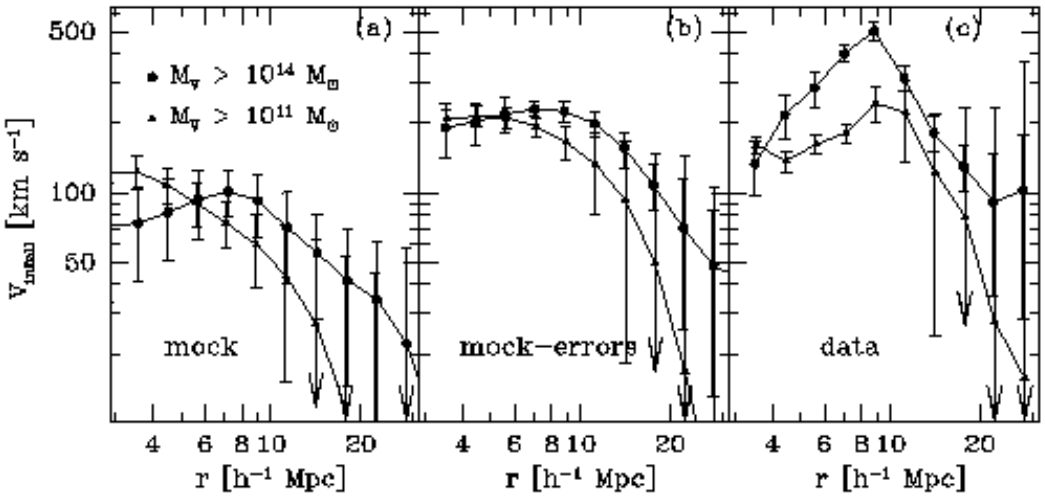

Fig. 7.— Panel a: Mean streaming peculiar velocity toward simulated groups for galaxies in the mock catalog. The results were derived using the same method applied to the data. Triangles correspond to groups with virial mass greater than 10^{11} $M_\odot$, and circles correspond to groups with virial mass greater than 10^{14} $M_\odot$. Panel b: same as panel a, but with distances measurements errors. Panel c: Mean streaming peculiar velocity of CPV onto UZC groups. The different symbols correspond to different ranges of group virial mass, as indicated in panel a. Errors are derived from the scatter in several mock catalogs.

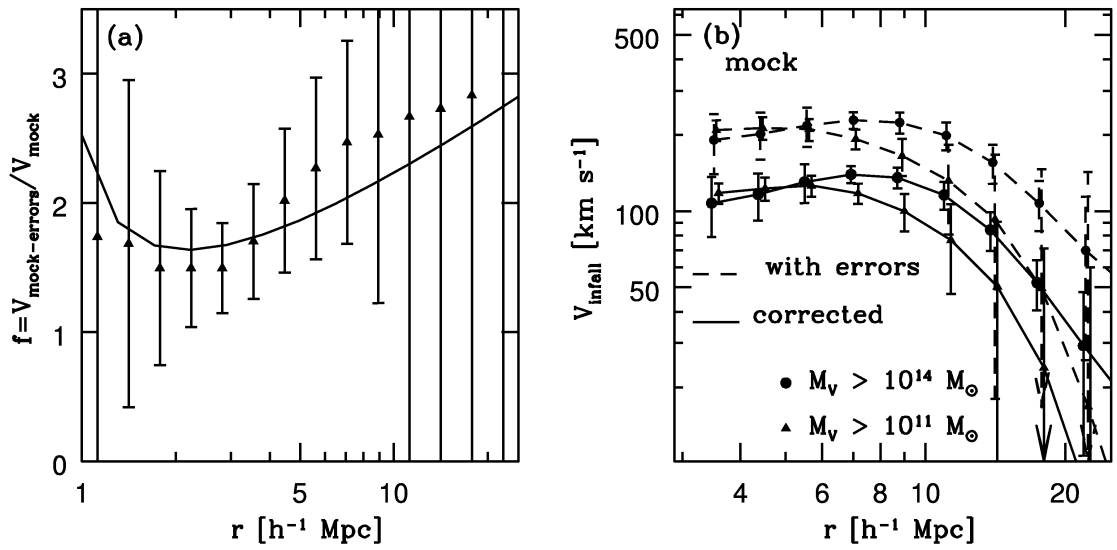

Fig. 8.— (a) The ratio, f, between the infall amplitude measured from the mock catalogs that include distance uncertainties and the infall amplitude of mock catalogs without errors (triangles). The solid line shows a fit to the measured values of f (see text). (b)Corrected mock infall velocities (solid lines) and infall velocities affected by distance uncertainties (dashed lines). Circles represent groups with masses greater than $10^{14}M_{\odot}$ and triangles represent groups more massive than $10^{11}M_{\odot}$. Errors are derived from the scatter in several mock catalogs.

8. Infall amplitude and mass overdensity

In this section we assume that the linear theory prediction that relates the integrated mass overdensity with an infall peculiar velocity is valid at distances greater than 5 h^{-1} Mpc. By doing this we can directly derive the mean integrated mass overdensity (δ) in a spherical volume centered on the groups. As discussed in the previous section, the results from the mock catalogs indicate that the effects of distance uncertainties must be corrected for in order to derive the actual mean infall velocities.

We apply the correction $f = V_{mock-errors}/V_{mock}$ to the infall velocities measured from the observational data (plotted in figure 5). Panel (a) of figure 9 shows the corrected mean infall amplitudes of the samples analyzed previously. The mean integrated mass overdensities shown in panel (b) are derived from the corrected infall velocities shown in panel a calculated using $V_{infall}(r) = -1/3 H_0 \Omega_0^{0.6} r\delta(r)$, where we have assumed a density parameter $\Omega = 0.3$

We have also corrected for distance errors on the inferred infall velocities of galaxies onto groups of different luminosity and virial mass ranges. We have accordingly applied a correction factor $f = V_{mock-errors}/V_{mock}$ to the infall velocities for which we note that the computed factors f for the different subsamples do not differ significantly. Figure 10 shows the corrected mean infall velocities and the corresponding mean integrated mass overdensities derived from linear theory for both the mock catalogs (panels a and b) and the observations (panels c and d) The mean corrected amplitude of infall velocities in the mock and observational data in the range of scales 5 h^{-1}Mpc $< r <$ 20 h^{-1} Mpc is $V \sim 100$ km s^{-1} for the low-luminosity groups, whereas the most luminous sample reachs infall velocities as high as 250 km s^{-1}. In the subsamples subdivided by virial mass we have a similar behavior: for the least massive groups, $V_{infall} \simeq 150$ km s^{-1}, whereas for the more massive systems, $V_{infall} \simeq 200$ km s^{-1}.

Table 1 lists the mean amplitude of infall velocities at 10h $^{-1}$ Mpc, V_{10}, obtained for the UZC and the mock catalog. The integrated mass overdensities derived within ~ 10 h^{-1} Mpc (δ_{10}) are shown in Table 2.

In order to test the reliability of the estimated overdensity values derived from linear theory, we have compared them with the actual mass overdensities computed in spherical volumes of radius 10 h $^{-1}$ Mpc in the simulations for different halo mass ranges. We obtain estimated overdensities in the mock catalogs in agreement with the actual values in the simulation, within the uncertainties, indicating the validity of the application of linear theory to the infall data to infer mass overdensities.

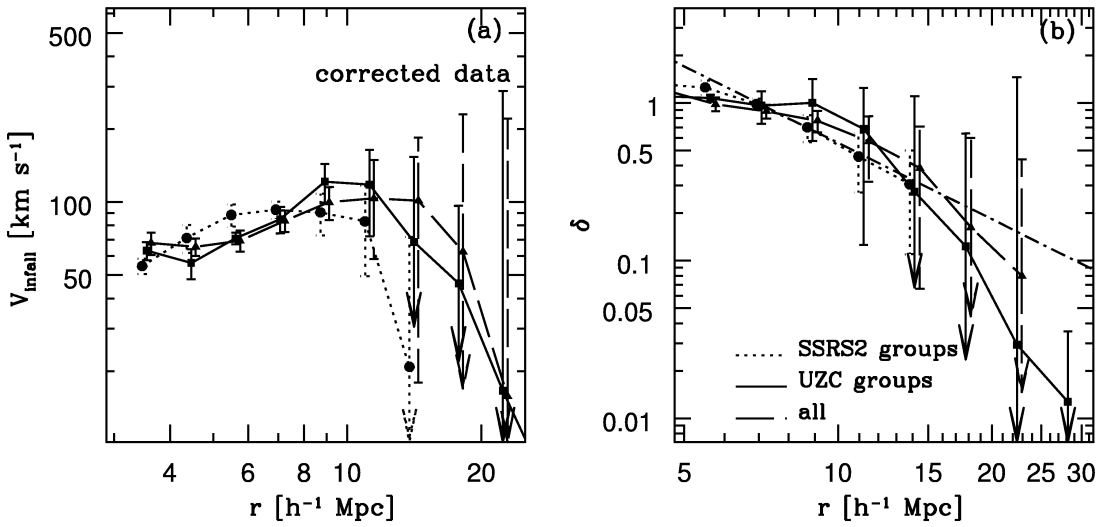

Fig. 9.— (a)Mean infall velocity of UZC (solid line), SSRS2 (dotted line) and the combined set of data (dashed line), corrected for distance uncertainties. (b) Integrated mass overdensity profile derived from linear theory; in both panels the same line type represents the same sample. The point-dashed line in panel b indicates the least-squares fit to results of the combined (UZC and SSRS2) sample. Errors are derived from the scatter in several mock catalogs.

Table 1. Infall amplitude at $10h^{-1}Mpc$

	Observational data		Mock data	
	V_{10}[km s^{-1}]	V_{10}[km s^{-1}]	V_{10}[km s^{-1}]	V_{10}[km s^{-1}]
	crude	corrected	crude	corrected
$\log_{10}(M_V/M_\odot) > 13.7$	375 ± 90	190 ± 45	210 ± 50	125 ± 30
$\log_{10}(M_V/M_\odot) < 13.7$	250 ± 90	155 ± 50	100 ± 35	65 ± 25
$\log_{10}(L_g/L_\odot) > 15$	450 ± 65	225 ± 30	350 ± 50	210 ± 30
$\log_{10}(L_g/L_\odot) < 15$	180 ± 90	110 ± 60	70 ± 30	50 ± 20

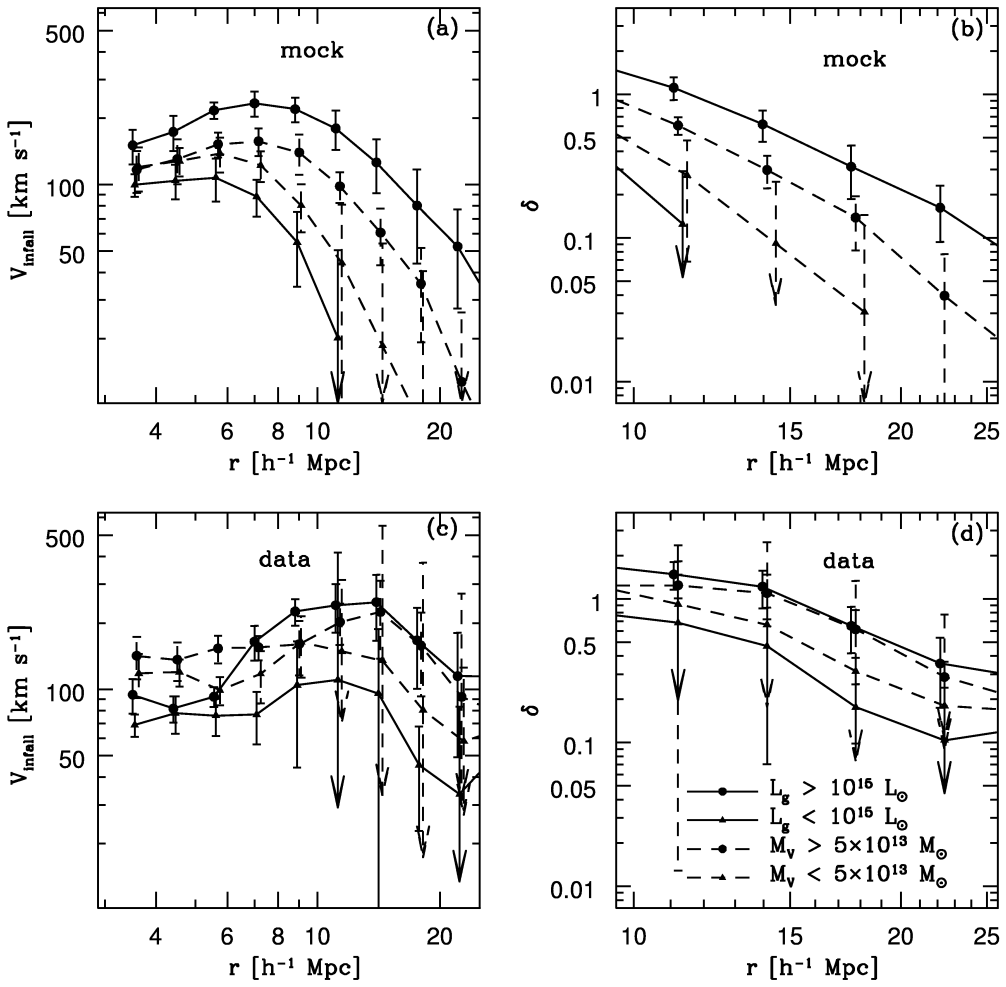

Fig. 10.— Results from mock (a,b) and observational (c,d) data. In all four panels, solid lines indicate subsamples divided by luminosity, whereas dashed lines indicate subsamples divided by virial mass. (a) Mock infall velocity corrected by distance errors. (b) Integrated mass overdensity as function of radius derived from linear theory. (c) Corrected infall velocity from observational data. (d) Integrated mass overdensity as function of radius derived from linear theory. Errors are derived from the scatter in several mock catalogs.

9. Discussion

We have analized the amplitude of the infall of galaxies onto groups and clusters in the nearby universe. Our study is based on the largest compilation of galaxy peculiar velocities to date and on a well defined and controlled sample of galaxy groups. The observational results were compared with numerical simulations, which include galaxy formation through semianalytical models and serve as a new test for the hierarchical models for structure formation within the ΛCDM scenario. The numerical simulations were also used to assess random and systematic errors in our measurements.

We summarize our findings as follows:

(i) We find a clear signature of infall of galaxies onto groups in a wide range of scales, 5 h^{-1}Mpc$< r <$ 30 h^{-1} Mpc. The amplitude of the infall velocities is of the order of few hundreds kilometers per second.

(ii) There is a significant dependence of the infall amplitude on group virial mass. For groups with $MV < 10^{13}$ $M_\odot$, we obtain $V_{infall} = 155 \pm 45$ km s^{-1}, whereas for $MV > 10^{13}$ $M_\odot$ a significantly larger amplitude of infall is observed, $V_{infall} = 190 \pm 40$ km s^{-1}.

(iii) In a similar fashion, the total group luminosity is a significant parameter that influences the infall amplitude. We find that groups with $L < 10^{15}$ $L_\odot$ have $V_{infall} = 110 \pm 50$ km s^{-1} whereas for $L > 10^{15}$ $L_\odot$ a value of $V_{infall} = 226 \pm 45$ km s^{-1} is measured. We observe a larger difference in the amplitude of infall velocities when dividing the group sample according to luminosity than to virial mass.

(iv) We obtain a similar behavior for the infall of galaxies onto groups in the numerical models and use the results from mock catalogs to measure the random errors inherent in our measurements and to correct the estimated infall amplitudes for systematic effects arising from distance measurement errors. The results for different virial mass and luminosity thresholds are consistent with those of the observational data, indicating that the models are suitable to reproduce the observations.

(v) We estimate integrated mass overdensities in spherical regions around galaxy groups. The resulting integrated mass overdensity in spheres of radius r is consistent with a power law of the form $\delta \sim (r/r_1)^{-1.6}$, with $r_1 \sim 10$ h^{-1} Mpc.

This research was supported by grants from Agencia Córdoba Ciencia, Secretaría de Ciencia y Técnica de la Universidad Nacional de Córdoba, Fundación Antorchas, and Agencia

Nacional de Promoción Científíca, Argentina. NP was supported by a FONDECYT grant no. 3040038, Chile. This work was partly supported by the ESO grant at PUC, Chile, and NSF grant AST-0307396 to RG.

REFERENCES

Benson, A.J., Lacey, C.G., Baugh, C.M.,Cole, S. & Frenk, C.S. 2002, MNRAS 333, 156

Bondi, H. 1974, MNRAS 107, 410

Cole, A.J., Lacey, C.G., Baugh, C.M. & Frenk, C.S. 2000, MNRAS 319, 168

Croft, R.A.C., Dalton, G.B. & Efstathiou, G. 1999, MNRAS, 305, 547

da Costa L.N. et al. 1998, A.J. 116, 1

Dale, D.A. & Giovanelli, R. 2000, in ASP Conf. Ser. vol. 201, *Cosmic Flows 1999*, ed. S. Courteau, M. Strauss & J. Willick (San Francisco: ASP), 25

Diaferio, A. & Geller, M.J. 1997, ApJ, 481, 633

Eke, V. R. et al. 2004, MNRAS, 355, 438

Ekhlom, T. & Teerikorpi, P. 1994, A&A, 284, 369

Falco, E.E. et al. 1999, PASP 111, 438

Giovanelli, R. & Haynes, M.P. 2002, ApJ, 571, L107

Giovanelli, R., Haynes, M.P., Herter, T., Vogt, N., da Costa, L.N., Freudling, W., Salzer, J.J. & Wegner, G. 1997a, AJ, 113, 22

Giovanelli, R., Haynes, M.P., Herter, T., Vogt, N., da Costa, L.N., Freudling, W., Salzer, J.J. & Wegner, G. 1997b, AJ113, 53

Gunn, J. E. 1978, *Observational Cosmology*, ed. M. Maeder, L. Martinet & G. Tamman (Sauveny: Geneva Obs.), 1

Gunn, J. E. & Gott, J. R. 1972, ApJ 176, 1

Haynes, M.P., Giovanelli, R., Salzer, J.J., Wegner, G., Freudling, W., da Costa, L.N.Herter, T. & Vogt, N.P. 1999, AJ, 117, 1668

Huchra, J.P. & Geller, M.J. 1982, ApJ, 257, 423

Maia, M.A.G., da Costa, L.N., & Latham, D.W.1989, ApJS 69, 809

Mathewson, D.S. & Ford, V.L. 1996, ApJS, 107, 97

Merchán, M.E., Maia, M.A,G., & Lambas,D 2000 ApJ, 544,2

Padilla, N. D. et al. 2004, MNRAS, 352, 211

Peebles, J.P.E. 1980, *The Large Scale Structure of the Universe*, (Princeton: Princeton University Press)

Ramella, M., Pisani, A., & Geller, M.J.,1997,AJ 113,483

Regös, E. & Geller, M.J. 1989, ApJ, 98, 3

Silk, J. 1974, ApJ 193, 525

Spergel, D. N. et al. 2003, ApJS, 148, 175

Tolman, R. C. 1934, Porc. Nat. Acad. Sci., 20, 164

Yahil, A. 1985, in ESO workshop on the *The Virgo Cluster of Galaxies*, ed. O. G. Richer & B. Bingelli (Garching: ESO), 359

Table 2. Integrated mass density within $10h^{-1}Mpc$

	Observational samples	Mock samples
	δ_{10}	δ_{10}
$\log_{10}(M_V/M_\odot) > 13.7$	1.2 ± 0.3	0.8 ± 0.2
$\log_{10}(M_V/M_\odot) < 13.7$	1.0 ± 0.4	0.5 ± 0.2
$\log_{10}(L_g/L_\odot) > 15$	1.5 ± 0.2	1.4 ± 0.2
$\log_{10}(L_g/L_\odot) < 15$	0.8 ± 0.4	0.3 ± 0.2